

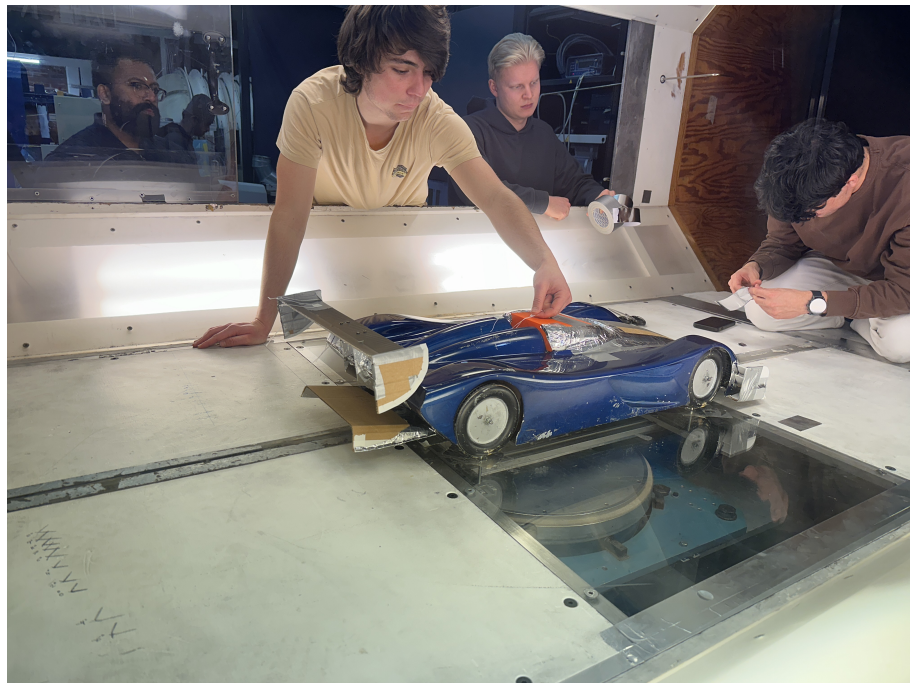


CHALMERS

Wind Tunnel Project Report

MTF236 - Road Vehicle Aerodynamics

Aerodynamics of Koenigsegg LMP 900



Group 7

Erwan Lecamp, Karthik Tapasi Himanth, Eeshan Ganla, Kannangarage Risira
Erantha Kannangara, Lars Petermeise, Syuen Khor, Valentin Da Silva

Contents

1	Introduction	2
2	Theoretical Background	3
2.1	Fundamentals of Aerodynamics for Racing Cars	3
2.2	Brief explanation of wind tunnel testing and scaling effects	3
3	Methodology	6
3.1	CFD Post-Processing	6
3.2	Wind Tunnel Setup	8
3.3	Measurement Techniques	9
3.4	Conducting the Reynolds sweep: procedure and data collection	9
3.5	Visualization techniques for aerodynamic evaluation	10
4	Results & Discussions	11
4.1	Interpretation of Reynolds sweep results	11
4.2	Analysis of measured forces	12
4.2.1	Drag Force and Downforce	14
4.2.2	Pitch Moment and Vehicle Balance	14
4.2.3	Effectiveness of downforce-generating devices	15
4.3	Aerodynamic coefficient calculations	15
4.4	Flow Visualization	15
4.4.1	Smoke Testing	16
4.4.2	String (Tuft) Testing	16
4.5	Comparison of results with pre-study hypotheses and literature	17
4.5.1	Front Splitter and front winglets	17
4.5.2	Effect of Front Splitter Length on Downforce	17
4.5.3	Rear Diffuser	18
4.5.4	Rear Wing	18
4.5.5	Ducktail Spoiler	18
4.5.6	Upper Body	18
5	Conclusion	19
5.1	Summary of Key Findings	19
5.2	Implications for Vehicle Aerodynamics and Design Optimization	19
5.3	Study Limitations	20
6	References	21
7	Appendix	22
7.1	Data Processing Code	22
8	Group Member Contributions	31

1 Introduction

The aerodynamic performance of a road vehicle significantly influences its efficiency, stability, and overall driving characteristics. As noted in [2], minimizing aerodynamic drag is essential for improving fuel efficiency and reducing emissions, making it a key consideration in modern vehicle design. Additionally, aerodynamic forces affect aspects such as handling, noise levels, and cooling efficiency, necessitating a comprehensive understanding of fluid flow behavior around vehicles. The study of vehicle aerodynamics remains a blend of experimental and computational approaches, with wind tunnel testing playing a crucial role in validating numerical simulations.



Figure 1: Wind tunnel model of the conceptual Koenigsegg LMP 900.

This report presents an aerodynamic investigation of a “conceptual Koenigsegg LMP 900” racing car using wind tunnel experimentation. The Koenigsegg LMP 900 is not an actual production or racing vehicle, but a scaled model designed for aerodynamic research. The Koenigsegg LMP 900 draws inspiration from high-performance racing vehicles designed for optimal down-force and minimal drag. With an advanced aerodynamic package, including diffusers, splitters, and other active aerodynamic components, it serves as an excellent subject for studying racing vehicle aerodynamics. The wind tunnel model used in this study is shown in Figure 1, which provides a scaled representation for controlled aerodynamic analysis. The study involves measuring key aerodynamic coefficients, visualizing flow patterns, and analyzing the impact of design modifications on drag, lift, and overall aerodynamic performance. By evaluating the effect of various add-ons on drag and lift characteristics, we aim to optimize vehicle performance under controlled conditions. The results are interpreted using fundamental aerodynamic principles, allowing us to correlate the observed changes with established theoretical concepts. Through this study, we gain insight into the practical applications of aerodynamic principles in automotive engineering, reinforcing the importance of a systematic approach to vehicle design.

2 Theoretical Background

2.1 Fundamentals of Aerodynamics for Racing Cars

Aerodynamic forces play a crucial role in the performance and stability of racing cars. The key aerodynamic forces acting on a race car are the drag force F_D , the downforce F_L and the lateral forces. These forces influence the car's speed and stability [2].

Drag force refers to the air resistance acting on a vehicle and is defined by Eq 1. It is a critical aerodynamic parameter, as it directly influences the vehicle's speed. A lower drag coefficient C_D reduces aerodynamic resistance, allowing for higher speeds and better acceleration. In racing applications, optimizing drag is essential to achieve an optimal balance between speed and stability [2].

$$F_D = \frac{1}{2}\rho V^2 AC_D \quad (1)$$

where:

- ρ is the air density (kg/m^3)
- V is the relative velocity of the air (m/s)
- A is the frontal area of the vehicle (m^2)
- C_D is the drag coefficient

Similarly, lift or downforce is defined by Eq 2, where C_L represents the lift coefficient (negative for downforce). Downforce plays a crucial role in maintaining tire grip and vehicle stability. At high speeds, increased downforce enhances cornering performance by improving traction and reducing the risk of sliding [2]. However, excessive downforce can lead to higher aerodynamic drag. Hence, it is important to achieve a balance between drag and downforce .

$$F_L = \frac{1}{2}\rho V^2 AC_L \quad (2)$$

The aerodynamic pitch moment about the center of the baseline is given by Eq 3, where C_M is the moment coefficient and L is the wheelbase length. The pitch moment M_y is a critical parameter in vehicle aerodynamics as it determines the distribution of aerodynamic forces between the front and rear axles. A positive pitch moment increases front lift, reducing front downforce, which can negatively affect steering response and stability. Conversely, a negative pitch moment increases front downforce, enhancing grip and handling. An effective aerodynamic design ensures a balanced pitch moment, optimizing vehicle performance under different driving conditions.

$$M_y = \frac{1}{2}\rho V^2 AC_M L \quad (3)$$

2.2 Brief explanation of wind tunnel testing and scaling effects

Wind tunnels are essential tools for studying aerodynamic performance under controlled conditions. They are classified into two types: *Open-Section Wind Tunnel* and *Closed-Section Wind Tunnel*.

In an *Open-Section Wind Tunnel*, air exits freely out of the tunnel after passing through the test section, whereas in the case of a *Closed-Section Wind Tunnel*, air is recirculated within a continuous loop. Compared to the open-section tunnels, closed-section tunnels minimize

external disturbances, ensure better airflow uniformity and allow for efficient energy usage by continuously recirculating the same air. Hence, at Chalmers, we use a closed-section wind tunnel, and its schematic diagram is shown in Figure 2.

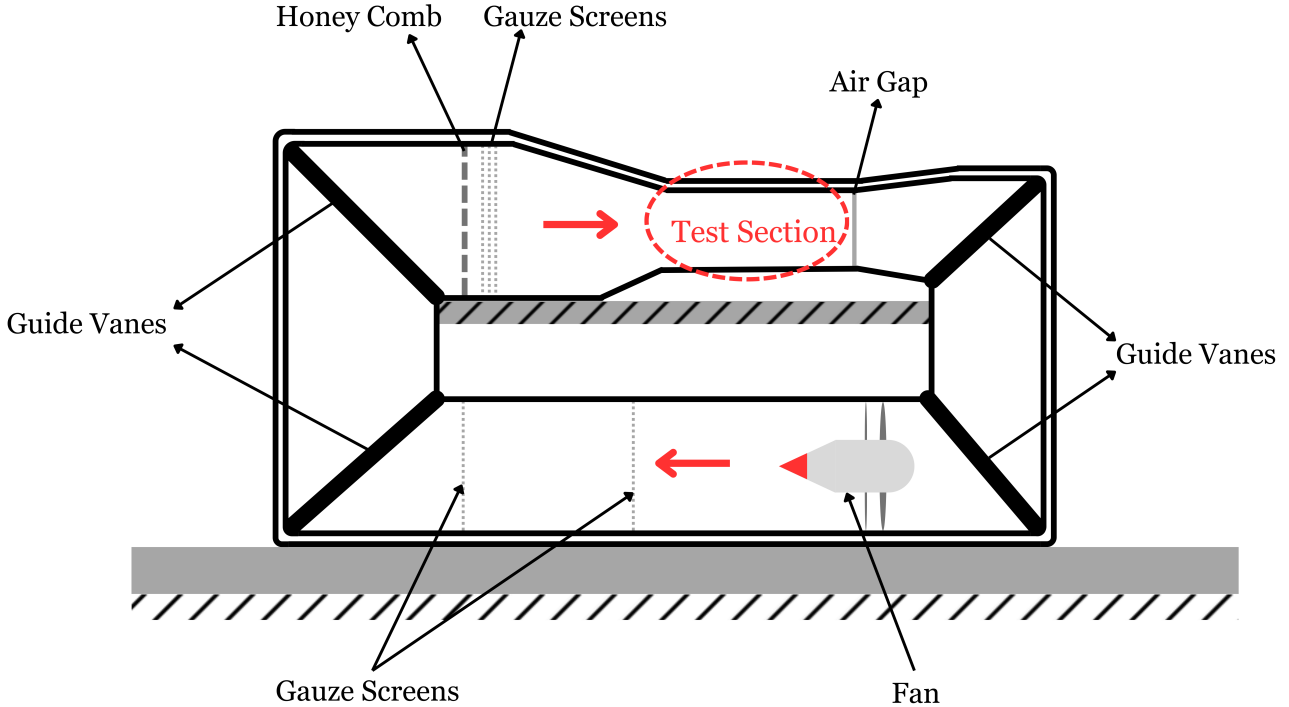


Figure 2: Chalmers Closed-Section Wind Tunnel

The Chalmers closed-section wind tunnel consists of several key components:

- **Test Section:** The area where the model is placed for aerodynamic evaluation, ensuring a uniform and steady flow over the test object.
- **Fan:** Drives airflow through the tunnel, maintaining controlled velocity for experiments.
- **Guide Vanes:** Help direct and smooth airflow to minimize turbulence before entering the test section.
- **Honeycomb and Gauze Screens:** Reduce flow disturbances, ensuring a steady, laminar approach to the test section.
- **Air Gap:** Aids in pressure equalization and minimizes unwanted flow disturbances.

Blockage Effects: In closed-section wind tunnels, the constrained test section results in a reduced cross-sectional area for airflow, causing the flow to accelerate more around the vehicle compared to real-world driving conditions. This higher velocity increases the dynamic pressure around the model, leading to overestimated aerodynamic forces such as lift and drag. Additionally, the dynamic pressure is often measured in the contraction section of the tunnel, which may not accurately represent the actual pressure around the vehicle in the test section. Hence, a dynamic pressure correction is necessary to obtain accurate coefficient values. The blockage ratio is defined as the ratio of the frontal area A to the cross-sectional area of the test section S . To correct for blockage effects, the measured aerodynamic coefficients must be adjusted using the empirical correction formula [3]:

$$C_{\text{true}} = C_{\text{measured}} \times \left(1 - \frac{A}{S}\right)^{1.288} \quad (4)$$

This correction ensures that the aerodynamic forces reflect real-world conditions by compensating for the confined airflow within the test section.

Scaling Effects: Since wind tunnel tests are conducted on scaled-down models rather than full-sized vehicles, it is essential to account for scaling effects to ensure accurate results. Key considerations include:

- **Reynolds Number Similarity:** Ensuring the test operates at an equivalent Reynolds number to match real-world aerodynamic behavior. In our case, we have a 1/5 scale model, so to achieve the same Reynolds number as in real life, we need to run the wind tunnel with a 5 times higher velocity, as shown by the expression for Reynolds Number [2]:

$$\text{Re} = \frac{\rho v L}{\mu} \quad (5)$$

- **Force and Moment Scaling:** Adjusting measured forces and moments to accurately predict full-scale vehicle performance, as aerodynamic forces depend on velocity, density, and model size. (Note: It is more reliable to use dimensionless coefficients such as C_L , C_D , and C_M , which allow comparison across different scales and test conditions without direct dependence on absolute force values) [2].
- **Geometric Similarity:** Maintaining proportional dimensions between the model and the actual vehicle to preserve flow characteristics.

Proper consideration of scaling effects helps to convert wind tunnel data into practical engineering insights for vehicle design.

3 Methodology

3.1 CFD Post-Processing

The initial step of this project involved analyzing a CFD simulation (using STAR-CCM+) of our baseline model, which had no modifications. This analysis aimed to identify the areas that already generate downforce and drag, as well as to locate regions where downforce could be further enhanced. To achieve this, we employed various visualization techniques, such as streamlines, vector, and scalar fields, along with different computational models to determine drag and lift forces.

We begin by analyzing the graphic that shows the distribution of the downforce along the vehicle in Figure 3:

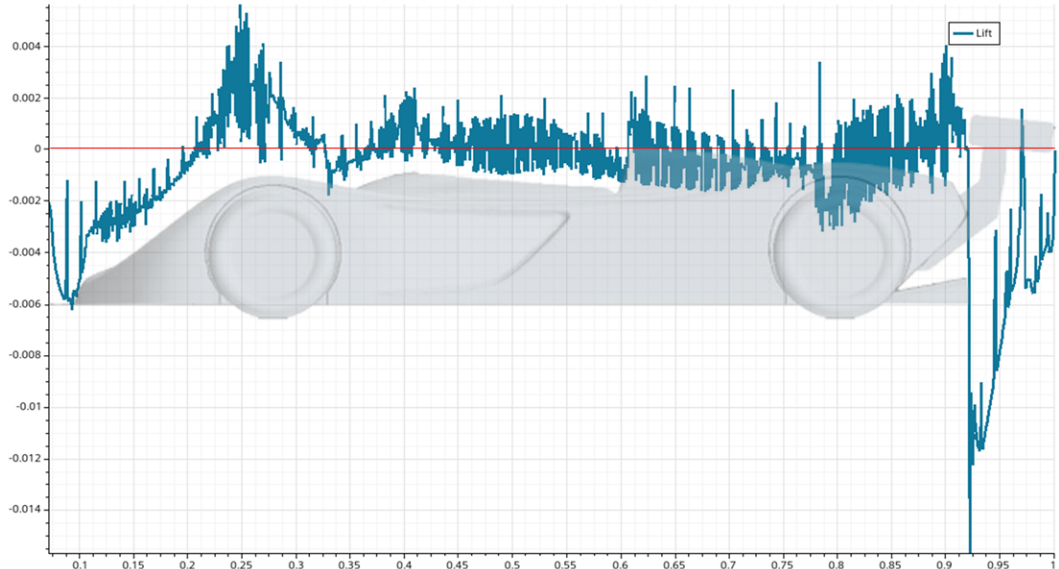


Figure 3: C_L distribution along the vehicle

As observed, the majority of the downforce is generated by the rear wing. We have a total lift coefficient of -0.828. Therefore, our initial focus is on the front of the car to explore potential enhancements. To do this, we analyze the pressure coefficient in Figure 4.

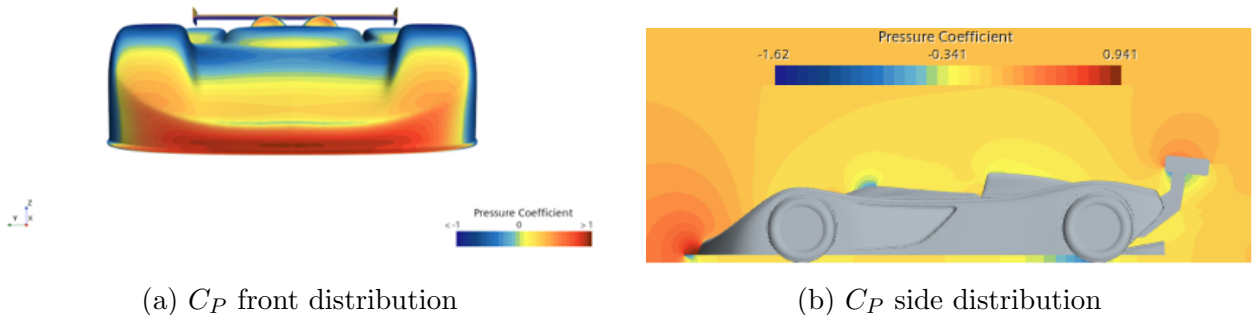


Figure 4: Pressure coefficient contour

It can be seen that the front stagnation area is relatively small. However, as discussed in the TTA lecture [1], we can leverage this area to generate more downforce at the front. By adding a larger splitter to the front, we can increase the high-pressure zone above the splitter (and low pressure under), which in turn pushes the front of the car downward, enhancing downforce.

Additionally, we can add front winglets to further increase downforce. These winglets should be placed on the outer edges, where the airflow accelerates. The winglets will decelerate the airflow, increasing the pressure on the surface. This increase in pressure generates downforce, which is the component of the force acting perpendicular to the surface. The projection of this force will be more or less normal to the ground, contributing to an increase in the overall downforce of the vehicle.

Subsequently, we analyzed the streamlines shown in Figure 5a to examine how the flow evolves around the car and to identify potential areas for performance improvement.

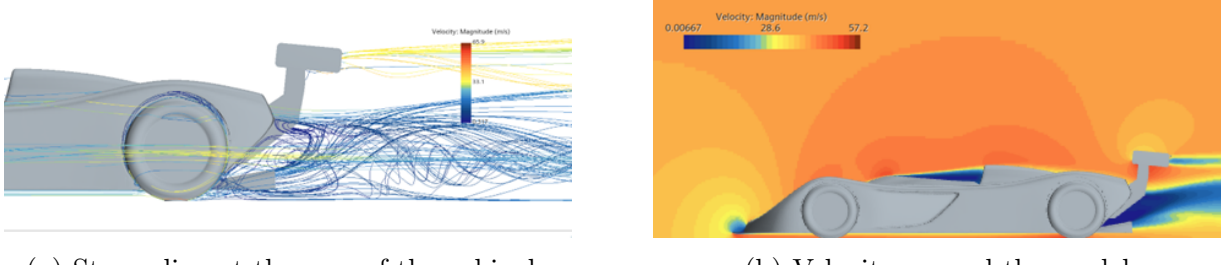


Figure 5: Rear analysis

The first area we aim to improve is the rear, where a significant depression is causing substantial drag. To address this, we decided to install a larger diffuser. This modification aims to reduce the shear layer between the high-speed airflow under the car and the low-speed airflow in the wake, thereby improving overall aerodynamic performance. Additionally, to optimize the flow over the car's upper surface, a 'ducktail' spoiler was proposed, functioning as an additional rear wing. The angle of this spoiler should be modest to avoid disrupting the flow beneath the main rear wing.

Following these modifications, we analyzed the rear wing, as illustrated in Figure 6, to further evaluate its performance and identify additional optimization opportunities.

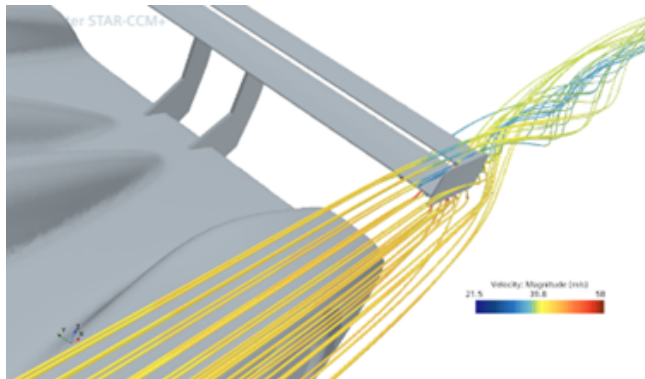


Figure 6: Vortex on the wing

Another point to improve is the side end of the rear wing, which generates vortices. To avoid this, we can add some winglets (like in aeronautics). To increase the performance of the rear wing, we aim to effectively separate the high-pressure area above the wing from the low-pressure area beneath it.

The last area we highlight is the top of the car, shown in figure 7:

Here in the middle of the car, we can see a recirculation area and another stagnation point that increases the drag. So we will close the area to avoid this increase in drag, even if our first objective is to increase downforce.

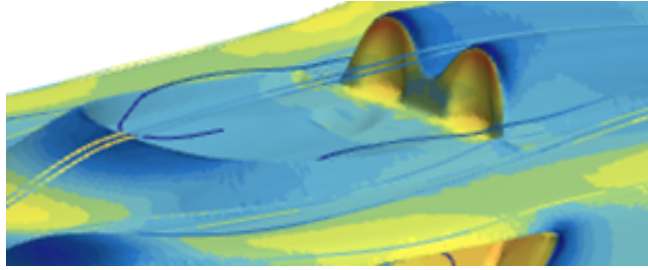


Figure 7: Top of the car

3.2 Wind Tunnel Setup

After completing the post-processing evaluation of our model, we began with the construction of the aerodynamic modifications. For this task, we gathered materials and tools such as paper, cardboard, duct tape, knives, scissors, and some 3D-printed parts. We built all the components highlighted in the CFD post-processing phase. Additionally, we reused two existing 3D-printed components: the top cover for the open section and two front winglets. Below, in Figure 8, you can see all the components described in the post-processing section, which we have built to increase the downforce of our vehicle.



(a) Top view



(b) Front assembly



(c) Ducktail



(d) Rear assembly

Figure 8: Aerodynamic devices.

After testing our planned modifications, we had enough time to build another configuration.

We decided to increase the area of the rear wing to observe how it would increase the downforce. In Figure 9, you can see the modified rear wing:



Figure 9: Extended rear wing

3.3 Measurement Techniques

We used four different methods to measure and analyze the flow around the car.

- A pitot probe was positioned at the beginning of the test section. This served as our velocity control to ensure that the set speed matched the actual velocity in the wind tunnel.
- To visualize the flow around the car, two methods were used. The first was tufts, which were placed on the car or attached to a long stick to observe the wake and side flows. Additionally, smoke was used to visualize flow patterns.
- The most crucial measurement tool was an external balance connected to the four wheels. This system provided numerical data on the forces acting on the model, including the pitch moment, the total lift force, and the distribution of lift between the front and rear wheels.

3.4 Conducting the Reynolds sweep: procedure and data collection

In our study, we conducted a Reynolds sweep to analyze the aerodynamic behavior of a model under varying flow conditions. By systematically adjusting the wind tunnel's velocity, we measured lift and drag coefficients to understand how these parameters change with the Reynolds number. Our goal was to identify the speed at which the drag coefficient and the lift coefficient converge to stable values, where further increases in the Reynolds number have minimal effect on the results.

3.5 Visualization techniques for aerodynamic evaluation

The extracted data was first converted to an Excel file and then post-processed using MATLAB® R2023b. The implemented script can be viewed in [7.1](#).

The measured fluid properties, as well as forces and moments, are extracted from the Excel table and saved together with the wind tunnel and model geometry. A separation is implemented between the measurements for the Reynolds sweep (baseline configuration) and the data from the applied measures. As the measures were applied sequentially without removal, the data must be corrected for the previously employed measures as well as for the blockage effect.

For the Reynolds sweep, C_D , C_L and the derived values for $C_{L,front}$ and $C_{L,rear}$ are plotted against the velocity. The relevant lift forces for the model's front and rear are calculated using the moment equilibrium method proposed in the lecture [\[3\]](#):

$$F_{LF} + F_{LR} = F_L \quad (6)$$

$$F_{LF} \cdot \frac{L_{WB}}{2} - F_{LR} \cdot \frac{L_{WB}}{2} = M_y \quad (7)$$

$$F_{LF} = \frac{F_L}{2} + \frac{M_y}{L_{WB}} \quad (8)$$

$$F_{LR} = \frac{F_L}{2} - \frac{M_y}{L_{WB}} \quad (9)$$

For the aerodynamic measurements, three further plots are generated. The two bar diagrams depict the absolute and relative effects on downforce, drag, and pitch.

According to the presumed coordinate system, a positive pitch moment induces a rotation that presses down the rear and lifts up the front of the vehicle.

In addition, a third graph is generated visualizing the force coefficients of the isolated measures, as well as their accumulation (label = '*Total*').

As presented in chapter [2](#), the dimensionless coefficients were calculated using the rearranged equations:

$$C_D = \frac{F_D}{\frac{\rho}{2} v^2 A} \quad (10)$$

$$C_L = \frac{F_L}{\frac{\rho}{2} v^2 A} \quad (11)$$

$$C_{M,p} = \frac{M_p}{\frac{\rho}{2} v^2 A L} \quad (12)$$

The final values are then visualized, while taking the blockage effects into consideration. The results are discussed in chapter [4](#).

4 Results & Discussions

4.1 Interpretation of Reynolds sweep results

The Reynolds sweep results, obtained from the reference vehicle configuration without any aerodynamic modifications, serve as a baseline for evaluating the aerodynamic performance. This configuration acts as a reference point, allowing analysis of how the aerodynamic coefficients of drag C_D , lift C_L , front lift $C_{L,front}$, and rear lift $C_{L,rear}$ vary across a range of velocities for the unmodified vehicle model, as illustrated in Figure 10. This can also determine the Reynolds number at which the simulation should run to ensure minimal variation in the values.

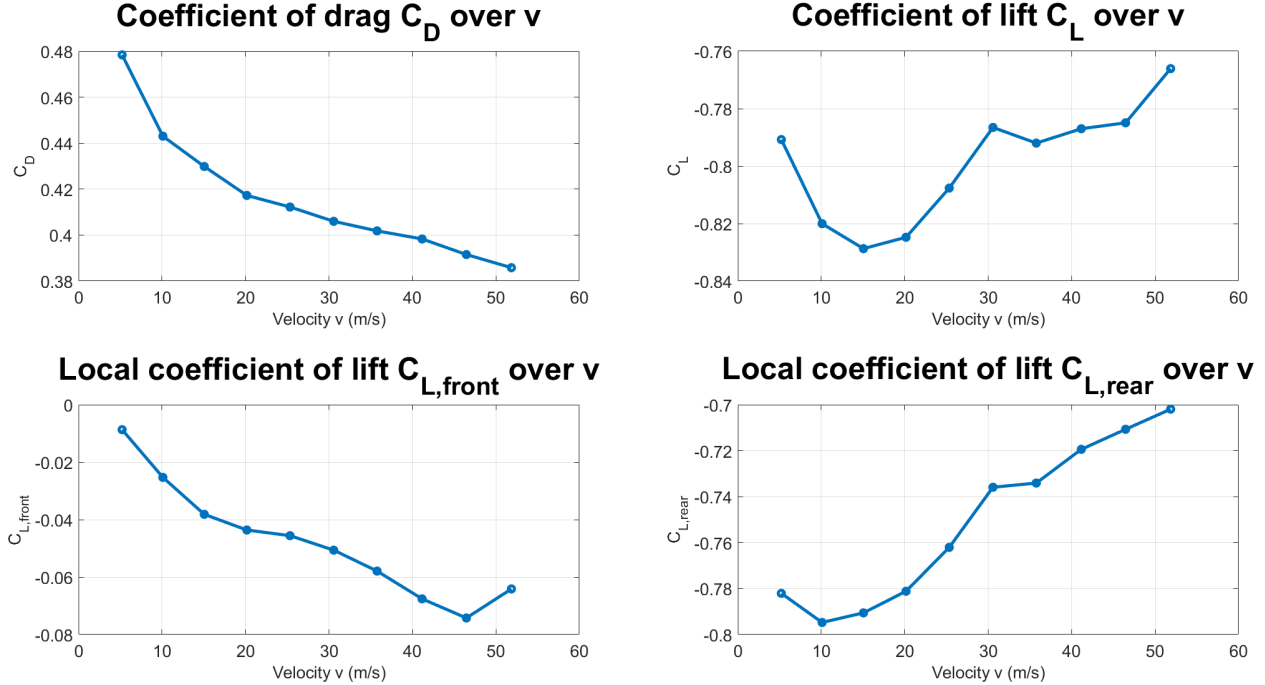


Figure 10: Variation of aerodynamic coefficients with velocity for the unmodified model

The graph of the coefficient of drag C_D shows that C_D decreases as velocity increases. As the velocity of the vehicle increases, the airflow along its surface, known as the boundary layer, undergoes a transition from laminar to turbulent. At lower velocities, the flow remains laminar. The fluid is smooth and parallel, causing low friction drag (viscous forces dominated), but the thin boundary layer tends to separate from the vehicle surface, resulting in a larger wake. This results in higher drag. As velocity increases, the flow transitions to a turbulent state. This causes higher friction drag as the fluid flow becomes unstable. However, the thicker boundary layer can attach to the vehicle surface for a longer distance before separation occurs. This results in a reduction in the wake size and therefore a reduction in the drag coefficient. Beyond a certain Reynolds number, the drag coefficient starts to decrease more slowly, where further increases in Re have less effect on C_D .

The coefficient of lift C_L represents the combined aerodynamic lift and downforce acting on both the front and rear sections of the vehicle. It is calculated as the sum of the front and rear lift coefficients:

$$C_L = C_{L,front} + C_{L,rear}$$

The graph of the front lift coefficient $C_{L,front}$ decreases as the velocity increases. The aerodynamic design of the front splitter effectively redirects airflow, which creates a downward force

on the front of the vehicle. This results in a pressure difference between the upper and lower surfaces of the splitter, generating downforce. As velocity increases, the airflow leads to a larger pressure difference between the upper and lower surfaces, causing more downforce to be generated. However, a slight increase in $C_{L,front}$ is observed at the end of the graph, possibly due to the front splitter detaching and vibrating at higher speeds, even making contact with the ground, creating an increase in lift.

In contrast, the graph of the rear lift coefficient $C_{L,rear}$ shows a non-linear pattern. At lower velocities, $C_{L,rear}$ decreases, indicating that the rear wing generates more downforce with increasing velocity, as downforce is proportional to the square of velocity ($F_d \propto v^2$). However, as velocity increases further, $C_{L,rear}$ begins to increase, showing a reduction in rear downforce. As airflow moves toward the rear, the boundary layer grows thicker and is more likely to transition to turbulent flow, leading to flow separation at the trailing edges. The separation of flow creates a low-pressure wake region behind the vehicle, reducing rear downforce and increasing the lift coefficient. At higher velocities, the boundary layer transitions to turbulence earlier, and the flow separation point moves forward along the rear surface, expanding the wake region behind the car. This reduces the pressure gradient across the vehicle, lowering downforce at the rear.

The nonlinear trend of $C_{L,front}$ and $C_{L,rear}$ suggests that these are potential areas in the unmodified design for aerodynamic optimization. Reducing flow separation and turbulence around the front and rear could help achieve more consistent and effective downforce generation across all speed ranges. Furthermore, at high speeds, the model vibrated and the front splitter started to detach from the model, thus the value of the C_L at high speed is not accurate and we will not take this value into account. Ultimately, the speed range of our testing was limited by the structural integrity of the model.

4.2 Analysis of measured forces

In the wind tunnel experiment, the aerodynamic forces acting on the vehicle were measured for both the baseline configuration and various aerodynamic modifications at a velocity of 35 m/s. The baseline refers to the unmodified vehicle and serves as a reference point. The modifications tested include the front (front splitter and front winglets), rear (diffuser and ducktail spoiler), winglets, upper body (engine bonnet and canopy), and an extended rear wing. Additionally, a "total" configuration was evaluated, combining all of the modifications to analyze the accumulated effect on aerodynamics.

The impact of these configurations on drag, downforce, and pitch moment is illustrated in Figures 11 and 12. Figure 11 represents the absolute effects of these changes, represented by the resulting dimensionless coefficients, which were calculated for the baseline with the respective additions. In addition, Figure 12 presents the percentage changes of the modifications relative to the baseline configuration. These results highlight the effectiveness of each aerodynamic element and provide insight into their interactions.

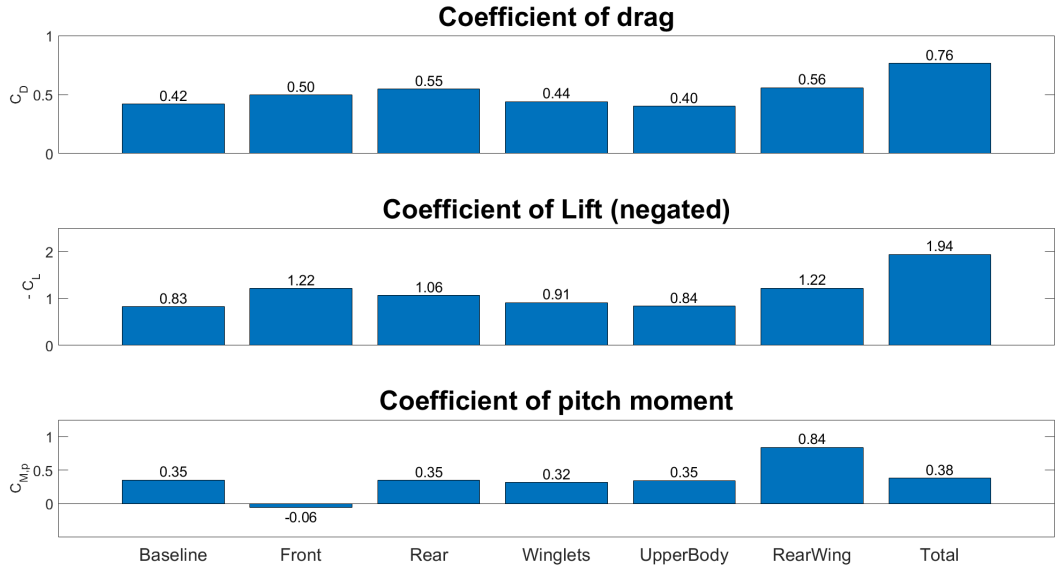


Figure 11: Coefficients of drag, downforce and pitch moment for various aerodynamic configurations

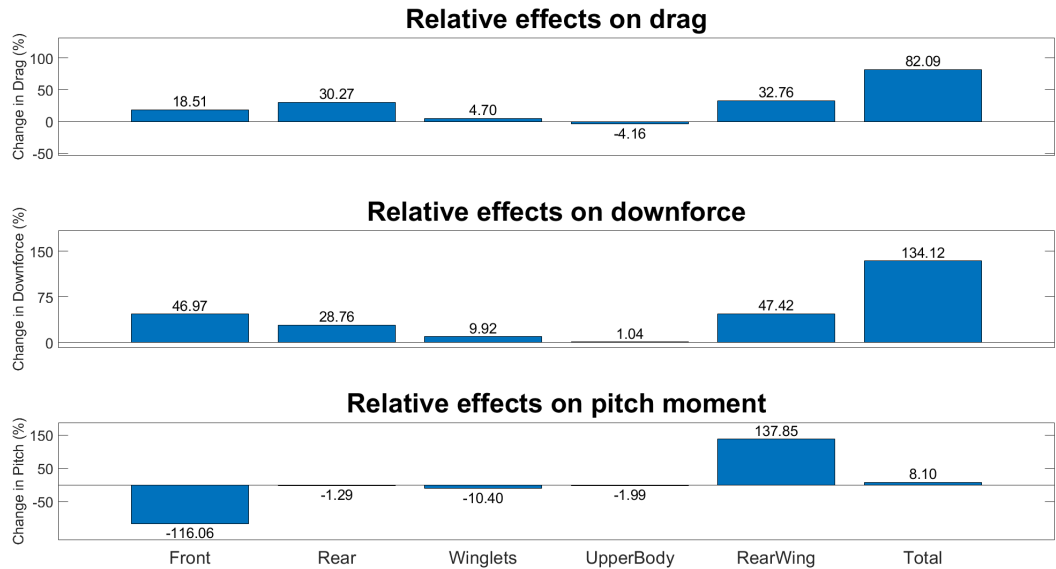


Figure 12: Percentage change in drag, downforce and pitch moment relative to the baseline configuration

First, we compare these coefficients with the ones we obtained during the post-processing session. At baseline, we have a lift coefficient of -0.83, which is remarkably close to the -0.828 from the CFD post-processing. For the coefficient of drag, a baseline value of 0.42 is measured, which differs from the CFD calculations of 0.359. These results show the limitations of simulative environments.

In the following, the effects of the employed measures are compared by a deviation from the baseline configuration in aerodynamic counts. One aerodynamic count represents a ΔC of 0.001 in the automotive context.

4.2.1 Drag Force and Downforce

The implementation of the front splitter and front winglet has a greater impact on downforce than drag. The downforce is improved by 390 counts. The splitter creates a high-pressure zone above it by reducing the incoming air velocity, while accelerating the airflow underneath. This effect reduces pressure and produces significant downforce. However, this modification causes to enlarge the frontal area and disturb the airflow, leading to an increase in aerodynamic resistance and increasing drag by 80 counts. Despite the additional frontal resistance causing higher form drag, the increase in downforce significantly improves front grip and overall stability, making this modification a beneficial trade-off.

The rear modifications, including the diffuser and ducktail spoiler, significantly contribute to both drag and downforce. While they increase drag by 130 counts due to the ducktail increasing the wake, they also improve downforce by 230 counts. This improvement is due to the higher pressure generated on top of the car by the ducktail and the acceleration of airflow beneath the car by the diffuser, which creates a suction effect that pulls the vehicle downward, enhancing stability.

The extended rear wing increases drag by 140 counts, as it generates a large high-pressure zone above the wing, while increasing downforce by 390 counts. The wake generated behind the wing causes additional separation losses, which contribute to drag. This improves vehicle stability at high speeds, but comes at the cost of increased drag due to the increased wake.

The winglets increase drag by 20 counts (not well designed; they create a stagnation point). While they contribute to drag, they also help to keep the main flow attached to the rear wing and separate the low and high pressure around it, preventing further mixing flow and improving overall aerodynamic efficiency.

In total, these rear modifications lead to an increase of 340 counts of drag. This highlights the trade-off between downforce and aerodynamic resistance. While the added downforce improves the vehicle's stability, especially at high speeds, the corresponding rise in drag reduces overall efficiency. However, the modifications to the upper body, which reduce drag by 20 counts, partially offset this drawback by streamlining the flow transition between the canopy and the rear section, delaying flow separation and reducing pressure losses.

4.2.2 Pitch Moment and Vehicle Balance

The interaction between the front and rear modifications affects the vehicle's pitch moment, which determines its overall balance. The front splitter and front winglets greatly improve downforce (+390 counts from the baseline) by accelerating airflow beneath the car and reducing pressure at the front. However, this leads to a negative pitch moment (-410 counts), as the increased suction at the front reduces rear grip. This effect is more noticeable when rear modifications are absent, as the earlier flow separation at the back causes a loss of rear downforce.

On the other hand, the rear wing adds significant downforce (+490 counts) at the rear, shifting the balance towards the rear and stabilizing the vehicle. This counters the front instability caused by the front splitter and front winglets. However, if the rear downforce outweighs the front, it can result in understeer.

In the total configuration, the modifications result in a slightly positive pitch moment (+30 counts), showing a more balanced aerodynamic load distribution. While the vehicle achieves greater overall stability, the rearward shift in balance may still lead to slight understeer.

In conclusion, these modifications improve stability and balance but come with compromises in drag and handling dynamics. This provides a basis for further analysis of downforce-generating devices and their role in optimizing aerodynamic performance and stability at high speeds.

4.2.3 Effectiveness of downforce-generating devices

The front splitter and front winglets significantly increase downforce at the front axle (+390 counts). However, as expected, it shifts the aerodynamic balance forward (-410 counts), reducing rear grip and confirming the need for rear modifications to maintain overall stability. The rear diffuser and ducktail spoiler enhance pressure recovery, leading to a notable increase in downforce (+230 counts). However, this improvement also generates a bigger wake, causing a rise in drag (+130 counts). The rear wing provides the most substantial boost to rear stability (+490 counts in pitch moment) by generating the highest downforce (+390 counts), although this comes at the cost of a significant drag increase (+140 counts). Meanwhile, the upper body modification smooths airflow transitions, reducing drag (-20 counts) without compromising stability.

4.3 Aerodynamic coefficient calculations

With the measured forces and the reference surface area, the aerodynamic coefficients C_D , C_L , $C_{L,front}$ and $C_{L,rear}$ of each modification are determined based on Eq 1, 2, 8 and 9 and plotted together with the baseline. It should be noted, that the derived values for the coefficients are calculated solely on the measure, meaning that all values have been subtracted by the respective baseline coefficient.

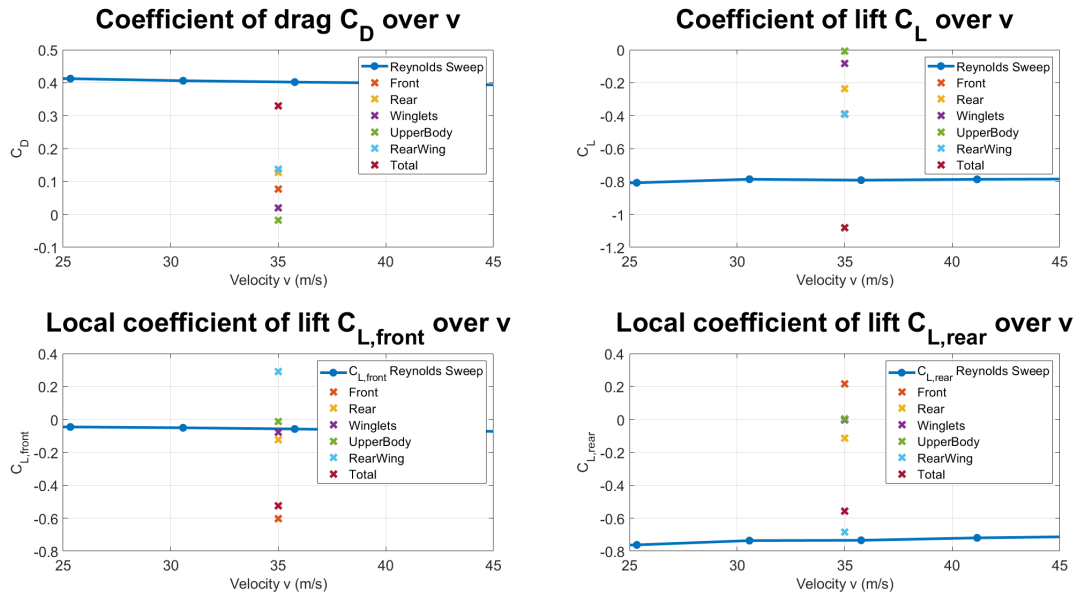


Figure 13: Aerodynamic coefficients of baseline configuration and all modifications

These coefficients are more useful than the forces because they are non-dimensional, making them easier to visualize and compare with the previous graphs. From the analysis, it is clear that the rear wing generates the highest downforce, while the upper body modification is the only modification that effectively reduces drag while improving downforce.

4.4 Flow Visualization

Flow visualization is critical for wind tunnel testing in the automotive sector. It allows engineers to assess and adjust the vehicle's aerodynamic performance. Flow visualization tools are used to depict airflow pathways, allowing us to discover high drag, turbulence, and flow separation, all of which have a direct impact on vehicle efficiency and stability.

4.4.1 Smoke Testing

Smoke testing involves adding a fine stream of smoke into the airflow surrounding a vehicle within the wind tunnel. The smoke traces the path of air across the vehicle's body, making it possible to observe airflow patterns, vortex formation, and flow separation with the naked eye. This technique helps to identify the regions of flow separation and the structure of turbulent wakes. During wind tunnel testing, turbulence wakes were observed behind the car. The image below illustrates the flow visualization around the rear wing.



Figure 14: Smoke test at the rear wing

4.4.2 String (Tuft) Testing

String testing involves sticking small, lightweight strings or tufts to the vehicle's surface at key aerodynamic locations. As air flows over the vehicle, the movement of these tufts provides a clear indication of the airflow behavior. Smooth and aligned strings indicate streamlined flow, while fluttering or chaotic tufts suggest turbulent or separated airflow.



Figure 15: String (or tuft) testing

4.5 Comparison of results with pre-study hypotheses and literature

4.5.1 Front Splitter and front winglets

The front splitter and front winglets are attached to the lower front section of the car to separate the airflow above and below the vehicle. They effectively manage the airflow beneath the car, reducing the pressure under the vehicle and creating a pressure difference (as described in Eq. 13). This pressure difference generates additional downforce, primarily on the front wheels, which improves front-end grip and stability. This is particularly useful at high speeds and during cornering. Additionally, they contribute to the ground effect, further increasing overall downforce and improving the vehicle's aerodynamic performance.

$$\Delta P = P_{\text{top}} - P_{\text{bottom}} - \frac{1}{2}\rho(V_{\text{bottom}}^2 - V_{\text{top}}^2) \quad (13)$$

Where:

- ΔP = Pressure difference
- P_{top} = Pressure at the top of the vehicle
- P_{bottom} = Pressure at the bottom of the vehicle
- ρ = Air density
- V_{bottom} = Velocity of air at the bottom of the vehicle
- V_{top} = Velocity of air at the top of the vehicle

The results obtained in the wind tunnel confirm our hypotheses.

4.5.2 Effect of Front Splitter Length on Downforce

The length of the front splitter, defined by how far it extends forward from the bumper, has a direct impact on the amount of downforce produced. As the splitter length increases, the surface area exposed to the pressure difference also increases, leading to a proportional rise in downforce, as described in Eq. 14 and 15.

$$F_{\text{down}} = \Delta P \cdot A_{\text{splitter}} \quad (14)$$

$$A_{\text{splitter}} = L \times W \quad (15)$$

Where:

- F_{down} = Downforce generated
- ΔP = Pressure difference (from Equation 13)
- A_{splitter} = Area of the splitter
- L = Length of splitter
- W = Width of splitter

A long splitter may come into contact with the ground at high speeds due to bending caused by excessive downforce, making such designs impractical. Furthermore, if the splitter is too close to the ground, the boundary layer of air underneath becomes thicker, reducing the effective passage for streamlined airflow. This can result in a condition where the smooth flow is disrupted, causing airflow stalling and turbulence. This turbulence causes airflow separation, which reduces downforce. To prevent airflow stalling and optimize downforce generation, it is crucial to ensure that the gap between the splitter and the ground exceeds the thickness of the boundary layer, as expressed in the following equation:

$$h_{\text{splitter}} > \delta_{\text{boundary layer}} \quad (16)$$

Where:

- h_{splitter} = ground clearance of the splitter
- $\delta_{\text{boundary layer}}$ = thickness of the boundary layer

4.5.3 Rear Diffuser

The diffuser accelerates the airflow as it exits from beneath the vehicle, resulting in reduced pressure underneath. This reduction increases the ground effect, thereby generating additional downforce and improving the vehicle's overall stability. As air flows beneath the car, the narrow underfloor space increases the velocity, which further decreases pressure. The higher pressure acting on the top of the car pushes it downward, effectively increasing the downforce.

4.5.4 Rear Wing

The rear wing generates significant downforce by creating a high-pressure area over its surface, effectively pressing the rear wheels onto the ground. This downforce enhances traction and stability, particularly during high-speed cornering.

4.5.5 Ducktail Spoiler

A ducktail spoiler reduces lift by modifying the airflow at the rear of the vehicle, as expected. Although it generates less downforce compared to a rear wing due to its smaller area, this modification is especially beneficial for maintaining control during high-speed cornering, as it improves stability.

4.5.6 Upper Body

If we look directly at the numerical results, we can detect something unusual: this device increases downforce and reduces drag. Theoretically, we would expect this update to decrease drag and increase lift, not downforce. In fact, with this update, we have accelerated flow on the top surface, which decreases pressure and theoretically results in a lift force. However, we need to examine how the flow evolves around the vehicle. The flow is now well-attached to the car, with less separation in the open area (which is now closed). This flow goes directly to the rear wing and the ducktail. The increase in lift by the upper body is countered by the increased downforce generated by the ducktail and the rear wing, thanks to better flow control.

5 Conclusion

5.1 Summary of Key Findings

This study analyzed and optimized the aerodynamic performance of a high-performance vehicle using a combination of CFD simulations and wind tunnel experiments. The results demonstrate the effectiveness of various aerodynamic modifications in enhancing downforce and managing drag.

Through CFD post-processing, critical areas for improvement were identified, including the front splitter, front winglets, rear diffuser, ducktail spoiler, and rear wing. The wind tunnel experiments validated these findings, confirming that modifications such as a larger front splitter and rear wing significantly increased downforce. However, these modifications also increased drag, demonstrating the trade-off between aerodynamic stability and efficiency.

The Reynolds number sweep demonstrated aerodynamic behavior at various velocities, showing that increasing velocity generally reduced drag coefficient due to boundary layer transition. However, nonlinear trends in front and rear lift coefficients indicated flow separation and turbulence effects near the rear wing, which were further analyzed through flow visualization techniques like tuft testing and smoke testing.

The aerodynamic modifications had a significant impact on vehicle balance. The front splitter effectively increased the front downforce but also induced a negative pitch moment, potentially destabilizing the rear. Conversely, the rear wing and diffuser improved rear downforce and high-speed stability at the cost of increased drag. The combined modifications resulted in a more balanced aerodynamic load distribution, although slight understeer remained.

In conclusion, while the aerodynamic modifications increased downforce and stability, they revealed the challenge of balancing drag and handling characteristics. Further adjustments, such as optimizing wing angles and integrating advanced flow control mechanisms, could help improve efficiency without compromising performance. These findings provide a foundation for future aerodynamic enhancements in high-performance vehicle design.

5.2 Implications for Vehicle Aerodynamics and Design Optimization

The findings of this study highlight the importance of balancing aerodynamic stability and efficiency in vehicle design. While increased downforce improves handling and cornering, the associated drag must be managed to maintain speed efficiency and fuel consumption. This trade-off is especially important in motorsport applications, where both downforce and straight-line speed are key performance factors. Future designs could incorporate adjustable components, such as active front splitters and adaptive rear wings, to allow dynamic control of aerodynamic forces depending on driving conditions. Additionally, adjusting the geometry of the rear wing and diffuser could enhance downforce generation while minimizing drag. Further improvements could be achieved by implementing advanced flow control techniques, such as vortex generators or boundary layer suction, to reduce flow separation and improve overall aerodynamic efficiency.

5.3 Study Limitations

Despite the valuable findings of this study, several limitations should be acknowledged. The CFD simulations relied on turbulence modeling assumptions, which may introduce uncertainties in predicting flow separation and wake behavior. Additionally, wind tunnel experiments were conducted at a reduced scale and Reynolds number, which may not fully replicate real-world aerodynamic conditions.

Besides, our model was not stable at high speeds as the front splitter started to detach while obtaining the Reynolds sweep results. The study also focused on steady-state aerodynamics, neglecting transient effects such as road-induced disturbances. To address these limitations, future research should include transient simulations, full-scale wind tunnel testing, and on-track validation.

By improving both experimental and computational methodologies, further advancements in vehicle aerodynamics and design optimization can be achieved, ultimately improving both performance and efficiency.

6 References

References

- [1] Hejdeste, M. (2025). *TTA Touring Car Racing*. Avantgarde Solutions AB.
- [2] Hucho, W. H. (1987). *Aerodynamics of Road Vehicles: From Fluid Mechanics to Vehicle Engineering*. Butterworth-Heinemann.
- [3] Vdovin, A. (2025). *Wind Tunnel Project Instruction*. Chalmers tekniska högskola.

7 Appendix

7.1 Data Processing Code

```
1 clc;
2 clear;
3 % Import data from the excel sheet and make sure the original column names
4 % are preserved
5 opts = detectImportOptions('WindTunnelData.xlsx', 'VariableNamingRule', ...
6     'preserve');
7
8 % Make sure all data is imported as data type 'string' in order to delete
9 % quotation marks
10 opts = setvartype(opts, 'string');
11
12 % Read data
13 data = readtable('WindTunnelData.xlsx', opts);
14
15 % Delete quotation marks from all entries
16 vars = data.Properties.VariableNames;
17 for i = 1:length(vars)
18     data.(vars{i}) = strrep(data.(vars{i}), '''', '');
19 end
20
21 % Convert numeric variables into 'double'
22 numericVars = {'dP', 'v', 'T', 'Pa', 'rho', 'nu', 'DragF', 'SideF', ...
23     'LiftF', 'rollM', 'pitchM', 'yawM'};
24 for i = 1:length(numericVars)
25     if ismember(numericVars{i}, vars)
26         data.(numericVars{i}) = str2double(data.(numericVars{i}));
27     end
28 end
29
30 % Extract names
31 Names = data.Name;
32
33 % Extract relevant variables
34 dP = data.dP;
35 v = data.v;
36 T = data.T;
37 Pa = data.Pa;
38 rho = data.rho;
39 nu = data.nu;
40 DragF = - data.DragF;
41 SideF = data.SideF;
42 LiftF = data.LiftF;
43 rollM = data.rollM;
44 pitchM = data.pitchM;
45 yawM = data.yawM;
46
47 % Save variables in the workspace
```

```

48 assignin('base', 'Names', Names);
49 assignin('base', 'dP', dP);
50 assignin('base', 'v', v);
51 assignin('base', 'T', T);
52 assignin('base', 'Pa', Pa);
53 assignin('base', 'rho', rho);
54 assignin('base', 'nu', nu);
55 assignin('base', 'DragF', DragF);
56 assignin('base', 'LiftF', LiftF);
57 assignin('base', 'pitchM', pitchM);

58 % Initialization of reference areas
59 A = 0.0576; % m2 (model frontal area)
60 S = 1.8 * 1.25; % m2 (test section area)
61 L = 0.51; % m (model wheelbase)

62 %% Visualize absolute effects of the implemented measures:
63 % Filter measures (no Reynolds sweep)
64 measure_indices = ~contains(Names, 'ReSwp');
65 measure_Names = Names(measure_indices);
66 measure_DragF = DragF(measure_indices);
67 measure_LiftF = LiftF(measure_indices);
68 measure_pitchM = pitchM(measure_indices);

69 % Find baseline index (ReSwp35)
70 baseline_idx = find(contains(Names, 'ReSwp35'));
71 baseline_DragF = DragF(baseline_idx);
72 baseline_LiftF = LiftF(baseline_idx);
73 baseline_pitchM = pitchM(baseline_idx);

74 % Correct measurements for single adjustments as well as blockage effect
75 % for dimensionless coefficients
76 c_Blockage = (1 - A/S)^1.288;

77 % Implement values for dimensionless coefficients
78 v_35 = 35; % m/s

79 % Identification of sweep data
80 sweep_indices = contains(Names, 'ReSwp');
81 sweep_v = v(sweep_indices);
82 sweep_rho = rho(sweep_indices);

83 % Use air density corresponding to v = 35 m/s from sweep data
84 rho_35 = interp1(sweep_v, sweep_rho, v_35, 'linear', 'extrap');
85 % Transform absolute forces to CD, CL
86 c_Force = 2 / (rho_35 * v_35^2 * A);
87 % Transform absolute moment to CM
88 c_Moment = 2 / (rho_35 * v_35^2 * A * L);

89 abs_Names = ["Baseline" ; "Front"; "Rear"; "Winglets"; "UpperBody"; ...

```

```

98 "RearWing"; "Total"];
99 abs_DragF = ([0 ; measure_DragF(1) - baseline_DragF; ...
100    measure_DragF(2) - measure_DragF(1); measure_DragF(6) - ...
101    measure_DragF(2); measure_DragF(7) - measure_DragF(6); ...
102    measure_DragF(8) - measure_DragF(7); measure_DragF(8) - ...
103    baseline_DragF] + baseline_DragF) .* (c_Blockage * c_Force);
104 abs_LiftF = ([0 ; measure_LiftF(1) - baseline_LiftF; ...
105    measure_LiftF(2) - measure_LiftF(1); measure_LiftF(6) - ...
106    measure_LiftF(2); measure_LiftF(7) - measure_LiftF(6); ...
107    measure_LiftF(8) - measure_LiftF(7); measure_LiftF(8) - ...
108    baseline_LiftF] + baseline_LiftF) .* (c_Blockage * c_Force);
109 abs_pitchM = ([0 ; measure_pitchM(1) - baseline_pitchM; ...
110    measure_pitchM(2) - measure_pitchM(1); measure_pitchM(6) - ...
111    measure_pitchM(2); measure_pitchM(7) - measure_pitchM(6); ...
112    measure_pitchM(8) - measure_pitchM(7); measure_pitchM(8) - ...
113    baseline_pitchM] + baseline_pitchM) .* (c_Blockage * c_Moment);
114
115 % Visualization of changes in DragF, LiftF und pitchM
116 figure;
117
118 % Ensure correct order
119 abs_Categories = categorical(abs_Names, abs_Names, 'Ordinal', true);
120
121 % Create indices for the x-position of the values
122 xPos = 1:length(abs_DragF);
123
124 subplot(3,1,1);
125 bar1 = bar(abs_Categories, abs_DragF);
126 xticks([])
127 ax1 = gca;
128 ax1.YAxis.FontSize = 16;
129 ylabel('C_D', 'FontSize', 16);
130 ylim([0 1]);
131 title('Coefficient of drag', 'FontSize', 30);
132
133 % Show values above bars, relevant for negative values
134 yPos = abs_DragF;
135 for i = 1:length(xPos)
136     if yPos(i) >= 0
137         va = 'bottom';
138     else
139         va = 'top';
140     end
141     text(xPos(i), yPos(i), num2str(yPos(i), '%.2f'), ...
142         'HorizontalAlignment', 'center', 'VerticalAlignment', ...
143         va, 'FontSize', 16);
144 end
145
146 subplot(3,1,2);
147 bar2 = bar(abs_Categories, - abs_LiftF);

```

```

148 xticks([])
149 ax2 = gca;
150 ax2.YAxis.FontSize = 16;
151 yticks([0 1 2])
152 ylabel('- C_L', 'FontSize', 16);
153 ylim([0 2.5]);
154 title('Coefficient of Lift (negated)', 'FontSize', 30);
155
156 % Show values above bars, relevant for negative values
157 yPos = -abs_LiftF;
158 for i = 1:length(xPos)
159     if yPos(i) >= 0
160         va = 'bottom';
161     else
162         va = 'top';
163     end
164     text(xPos(i), yPos(i), num2str(yPos(i), '%.2f'), ...
165          'HorizontalAlignment', 'center', 'VerticalAlignment', ...
166          va, 'FontSize', 16);
167 end
168
169 subplot(3,1,3);
170 bar3 = bar(abs_Categories, abs_pitchM);
171 ax3 = gca;
172 ax3.XAxis.TickLength = [0 0];
173 ax3.XAxis.FontSize = 20;
174 ax3.YAxis.FontSize = 16;
175 yticks([0 0.5 1])
176 ylabel('C_{M,p}', 'FontSize', 16);
177 ylim([-0.5 1.25]);
178 title('Coefficient of pitch moment', 'FontSize', 30);
179
180 % Show values above bars, relevant for negative values
181 yPos = abs_pitchM;
182 for i = 1:length(xPos)
183     if yPos(i) >= 0
184         va = 'bottom';
185     else
186         va = 'top';
187     end
188     text(xPos(i), yPos(i), num2str(yPos(i), '%.2f'), ...
189          'HorizontalAlignment', 'center', 'VerticalAlignment', va, ...
190          'FontSize', 16);
191 end
192
193 %% Visualize relative effects of the implemented measures:
194 % Filter measures (no Reynolds sweep)
195 measure_indices = ~contains(Names, 'ReSwp');
196 measure_Names = Names(measure_indices);
197 measure_DragF = DragF(measure_indices);

```

```

198 measure_LiftF = LiftF(measure_indices);
199 measure_pitchM = pitchM(measure_indices);
200
201 % Correct measurements for single adjustments as well as blockage effect
202 rel_Names = ["Front"; "Rear"; "Winglets"; "UpperBody"; "RearWing"; ...
203     "Total"];
204 rel_DragF = [measure_DragF(1) - baseline_DragF; measure_DragF(2) - ...
205     measure_DragF(1); measure_DragF(6) - measure_DragF(2); ...
206     measure_DragF(7) - measure_DragF(6); measure_DragF(8) - ...
207     measure_DragF(7); measure_DragF(8) - baseline_DragF] ...
208     ./ baseline_DragF * 100;
209 rel_LiftF = [measure_LiftF(1) - baseline_LiftF; measure_LiftF(2) - ...
210     measure_LiftF(1); measure_LiftF(6) - measure_LiftF(2); ...
211     measure_LiftF(7) - measure_LiftF(6); measure_LiftF(8) - ...
212     measure_LiftF(7); measure_LiftF(8) - baseline_LiftF] ...
213     ./ baseline_LiftF * 100;
214 rel_pitchM = [measure_pitchM(1) - baseline_pitchM; measure_pitchM(2) - ...
215     measure_pitchM(1); measure_pitchM(6) - measure_pitchM(2); ...
216     measure_pitchM(7) - measure_pitchM(6); measure_pitchM(8) - ...
217     measure_pitchM(7); measure_pitchM(8) - baseline_pitchM] ...
218     ./ baseline_pitchM * 100;
219
220 % Visualization of changes in DragF, LiftF und pitchM
221 figure;
222
223 % Ensure correct order
224 rel_Categories = categorical(rel_Names, rel_Names, 'Ordinal', true);
225
226 % Create indices for the x-position of the values
227 xPos = 1:length(rel_DragF);
228
229 subplot(3,1,1);
230 bar1 = bar(rel_Categories, rel_DragF);
231 xticks([])
232 ax1 = gca;
233 ax1.YAxis.FontSize = 16;
234 ylabel('Change in Drag (%)', 'FontSize', 16);
235 ylim([min(rel_DragF)-50 max(rel_DragF)+50]);
236 title('Relative effects on drag', 'FontSize', 30);
237
238 % Show values above bars, relevant for negative values
239 yPos = rel_DragF;
240 for i = 1:length(xPos)
241     if yPos(i) >= 0
242         va = 'bottom';
243     else
244         va = 'top';
245     end
246     text(xPos(i), yPos(i), num2str(yPos(i), '%.2f'), ...
247         'HorizontalAlignment', 'center', 'VerticalAlignment', ...

```

```

248     va, 'FontSize', 16);
249 end
250
251 subplot(3,1,2);
252 bar2 = bar(rel_Categories, rel_LiftF);
253 xticks([])
254 ax2 = gca;
255 ax2.YAxis.FontSize = 16;
256 yticks([0 75 150])
257 ylabel('Change in Downforce (%)', 'FontSize', 16);
258 ylim([min(rel_LiftF)-10 max(rel_LiftF)+50]);
259 title('Relative effects on downforce', 'FontSize', 30);
260
261 % Show values above bars, relevant for negative values
262 yPos = rel_LiftF;
263 for i = 1:length(xPos)
264     if yPos(i) >= 0
265         va = 'bottom';
266     else
267         va = 'top';
268     end
269     text(xPos(i), yPos(i), num2str(yPos(i), '%.2f'), ...
270           'HorizontalAlignment', 'center', 'VerticalAlignment', ...
271           va, 'FontSize', 16);
272 end
273
274 subplot(3,1,3);
275 bar3 = bar(rel_Categories, rel_pitchM);
276 ax3 = gca;
277 ax3.XAxis.TickLength = [0 0];
278 ax3.XAxis.FontSize = 20;
279 ax3.YAxis.FontSize = 16;
280 yticks([-50 50 150])
281 ylabel('Change in Pitch (%)', 'FontSize', 16);
282 ylim([min(rel_pitchM)-50 max(rel_pitchM)+50]);
283 title('Relative effects on pitch moment', 'FontSize', 30);
284
285 % Show values above bars, relevant for negative values
286 yPos = rel_pitchM;
287 for i = 1:length(xPos)
288     if yPos(i) >= 0
289         va = 'bottom';
290     else
291         va = 'top';
292     end
293     text(xPos(i), yPos(i), num2str(yPos(i), '%.2f'), ...
294           'HorizontalAlignment', 'center', 'VerticalAlignment', ...
295           va, 'FontSize', 16);
296 end

```

```

298 %% Visualize the Reynolds sweep:
299 % We should include a reference horizontal line in all graphs visualizing
300 % the point from which on there is less change in the behaviour over
301 % velocity
302
303 % Identification of sweep data
304 sweep_indices = contains(Names, 'ReSwp');
305 sweep_v = v(sweep_indices);
306 sweep_DragF = DragF(sweep_indices);
307 sweep_LiftF = LiftF(sweep_indices);
308 sweep_pitchM = pitchM(sweep_indices);
309 sweep_rho = rho(sweep_indices);
310
311 % Calculate coefficient of drag CD
312 CD = 2 * sweep_DragF ./ (sweep_rho .* sweep_v.^2 * A);
313 % Correct for blockage-effect
314 CD_true = CD .* (1 - A/S)^1.288;
315
316 % Calculate coefficient of lift CL
317 CL = 2 * sweep_LiftF ./ (sweep_rho .* sweep_v.^2 * A);
318 % Correct for blockage-effect
319 CL_true = CL .* (1 - A/S)^1.288;
320
321 % Calculation of LiftF_front und LiftF_rear from force & moment equilibrium
322 % For reference take a look at the wind tunnel lab presentation.
323 % Calculate the lift force at the front axis
324 LiftF_front = (sweep_LiftF + (2 * sweep_pitchM) ./ L) / 2;
325
326 % Calculate the lift force at the rear axis
327 LiftF_rear = sweep_LiftF - LiftF_front;
328
329 % Calculate coefficients of lift on both axes
330 CL_front = 2 * LiftF_front ./ (sweep_rho .* sweep_v.^2 * A);
331 CL_rear = 2 * LiftF_rear ./ (sweep_rho .* sweep_v.^2 * A);
332
333 % Correct for blockage-effect
334 CL_front_true = CL_front .* (1 - A/S)^1.288;
335 CL_rear_true = CL_rear .* (1 - A/S)^1.288;
336
337 % Plot the coefficients over the velocity (Second Figure)
338 figure;
339 subplot(2,2,1);
340 plot(sweep_v, CD_true, '-o', 'LineWidth', 3);
341 ax = gca;
342 ax.XAxis.FontSize = 16;
343 ax.YAxis.FontSize = 16;
344 xlabel('Velocity v (m/s)', 'FontSize', 16);
345 ylabel('C_D', 'FontSize', 16);
346 title('Coefficient of drag C_D over v', 'FontSize', 30);
347 grid on;

```

```

348 subplot(2,2,2);
349 plot(sweep_v, CL_true, '-o', 'LineWidth', 3);
350 ax = gca;
351 ax.XAxis.FontSize = 16;
352 ax.YAxis.FontSize = 16;
353 xlabel('Velocity v (m/s)', 'FontSize', 16);
354 ylabel('C_L', 'FontSize', 16);
355 title('Coefficient of lift C_L over v', 'FontSize', 30);
356 grid on;
357
358 subplot(2,2,3);
359 plot(sweep_v, CL_front_true, '-o', 'LineWidth', 3);
360 ax = gca;
361 ax.XAxis.FontSize = 16;
362 ax.YAxis.FontSize = 16;
363 xlabel('Velocity v (m/s)', 'FontSize', 16);
364 ylabel('C_{L,front}', 'FontSize', 16);
365 title('Local coefficient of lift C_{L,front} over v', 'FontSize', 30);
366 grid on;
367
368 subplot(2,2,4);
369 plot(sweep_v, CL_rear_true, '-o', 'LineWidth', 3);
370 ax = gca;
371 ax.XAxis.FontSize = 16;
372 ax.YAxis.FontSize = 16;
373 xlabel('Velocity v (m/s)', 'FontSize', 16);
374 ylabel('C_{L,rear}', 'FontSize', 16);
375 title('Local coefficient of lift C_{L,rear} over v', 'FontSize', 30);
376 grid on;
377
378 %% Create third figure with measures data at 35 m/s
379 % Assume constant velocity and air density at 35 m/s
380 v_35 = 35; % m/s
381 % Use air density corresponding to v = 35 m/s from sweep data
382 rho_35 = interp1(sweep_v, sweep_rho, v_35, 'linear', 'extrap');
383
384 % subtract baseline from Total for these plots
385 abs_DragF2 = abs_DragF - [zeros(6,1); baseline_DragF];
386 abs_LiftF2 = abs_LiftF - [zeros(6,1); baseline_LiftF];
387 abs_pitchM2 = abs_pitchM - [zeros(6,1); baseline_pitchM];
388
389 % Calculate CD, CL, CL_front, CL_rear for each measure using abs_* arrays
390 CD_measures = 2 * abs_DragF2 ./ (rho_35 * v_35^2 * A);
391 CL_measures = 2 * abs_LiftF2 ./ (rho_35 * v_35^2 * A);
392
393 % Compute LiftF_front and LiftF_rear from abs_LiftF and abs_pitchM
394 LiftF_front_measures = (abs_LiftF2 + (2 * abs_pitchM2) / L) / 2;
395 LiftF_rear_measures = abs_LiftF2 - LiftF_front_measures;
396
397
```

```

398 % Compute CL_front and CL_rear
399 CL_front_measures = 2 * LiftF_front_measures ./ (rho_35 * v_35^2 * A);
400 CL_rear_measures = 2 * LiftF_rear_measures ./ (rho_35 * v_35^2 * A);
401
402 % Prepare legends using abs_Names
403 measure_legends = cellstr(abs_Names(2:end));
404
405 % Plot the coefficients over the velocity (Third Figure)
406 figure;
407 subplot(2,2,1);
408 plot(sweep_v, CD_true, '-o', 'LineWidth', 3);
409 hold on;
410 for i = 2:length(abs_Names)
411     plot(v_35, CD_measures(i), 'x', 'MarkerSize', 10, 'LineWidth', 3);
412 end
413 ax = gca;
414 ax.XAxis.FontSize = 16;
415 ax.YAxis.FontSize = 16;
416 xlabel('Velocity v (m/s)', 'FontSize', 16);
417 ylabel('C_D', 'FontSize', 16);
418 xlim([25 45]);
419 title('Coefficient of drag C_D over v', 'FontSize', 30);
420 legend_entries = ['Reynolds Sweep'; measure_legends];
421 legend(legend_entries, 'FontSize', 14);
422 grid on;
423
424 subplot(2,2,2);
425 plot(sweep_v, CL_true, '-o', 'LineWidth', 3);
426 hold on;
427 for i = 2:length(abs_Names)
428     plot(v_35, CL_measures(i), 'x', 'MarkerSize', 10, 'LineWidth', 3);
429 end
430 ax = gca;
431 ax.XAxis.FontSize = 16;
432 ax.YAxis.FontSize = 16;
433 xlabel('Velocity v (m/s)', 'FontSize', 16);
434 ylabel('C_L', 'FontSize', 16);
435 xlim([25 45]);
436 title('Coefficient of lift C_L over v', 'FontSize', 30);
437 legend_entries = ['Reynolds Sweep'; measure_legends];
438 legend(legend_entries, 'FontSize', 14);
439 grid on;
440
441 subplot(2,2,3);
442 plot(sweep_v, CL_front_true, '-o', 'LineWidth', 3);
443 hold on;
444 for i = 2:length(abs_Names)
445     plot(v_35, CL_front_measures(i), 'x', 'MarkerSize', 10, ...
446           'LineWidth', 3);
447 end

```

```

448 ax = gca;
449 ax.XAxis.FontSize = 16;
450 ax.YAxis.FontSize = 16;
451 xlabel('Velocity v (m/s)', 'FontSize', 16);
452 ylabel('C_{L,front}', 'FontSize', 16);
453 xlim([25 45]);
454 title('Local coefficient of lift C_{L,front} over v', 'FontSize', 30);
455 legend_entries = ['C_{L,front} Reynolds Sweep'; measure_legends];
456 legend(legend_entries, 'FontSize', 14);
457 grid on;
458
459 subplot(2,2,4);
460 plot(sweep_v, CL_rear_true, '-o', 'LineWidth', 3);
461 hold on;
462 for i = 2:length(abs_Names)
463     plot(v_35, CL_rear_measures(i), 'x', 'MarkerSize', 10, 'LineWidth', 3);
464 end
465 ax = gca;
466 ax.XAxis.FontSize = 16;
467 ax.YAxis.FontSize = 16;
468 xlabel('Velocity v (m/s)', 'FontSize', 16);
469 ylabel('C_{L,rear}', 'FontSize', 16);
470 xlim([25 45]);
471 title('Local coefficient of lift C_{L,rear} over v', 'FontSize', 30);
472 legend_entries = ['C_{L,rear} Reynolds Sweep'; measure_legends];
473 legend(legend_entries, 'FontSize', 14);
474 grid on;

```

8 Group Member Contributions

Below are all contributions listed, that have been done by the group members.

Erwan Lecamp I have worked on different parts of the project throughout its duration: First, I participated in the post-processing session and collaborated with some colleagues on the short analysis presentation for improvement (Lars, Valentin, Karthik).

During the building session, I built various elements, including the duck tail, front splitter, and diffuser.

During the wind tunnel session, I worked on preparing the model by mounting the different elements on the car and ensuring we had enough fixations with Valentin. I was also responsible for controlling the stability of the model during the tests and performing flow visualization with the tuft stick.

For the report, I read the entire document and discussed and add improvements with other group members (I mainly clarified and corrected certain phrases in the results section). I was responsible for writing the whole methodology section and contributed to the introduction. I also participated in the reflection and drafting of the Reynolds sweep analysis with Valentin and Syuen. Lastly, I add Upper body results analysis in the Comparison of results with pre-study hypotheses and literature part.

For the presentation, I prepared the oral presentation, created the PowerPoint slides (The content, not the appearance of the power point.), and decided on the key ideas to highlight during the presentation. I also conveyed the presentation with Risira.

Eeshan Ganla I was present for all the mandatory tasks and sessions. I prepared some of the streamlines plots along with Karthik during the post processing session. I also helped with the rear section modifications and contributed to the initial presentation during the building session.

During the wind tunnel session, I was involved in the preparation of all the components and I prepared the tufts and placed them on critical areas to observe the flow patterns. For the final presentation, I collaborated with Erwan and Karthik to prepare some of the slides. Additionally, I reviewed and edited the report to improve the language and ensure its accuracy.

Kannangarage Risira Erantha Kannangara I was present for all of the mandatory tasks and sessions. I participated in the discussion session that agreed to apply the car's aerodynamic improvements. I make proposals for aerodynamic surfaces that can be applied based on CFD post-processing data. During the wind tunnel session, I assisted in preparing and attaching aerodynamic components to the car. I am mostly responsible for building and mounting the rear wing. I obtained aid from my college when mounting the rear wing to the vehicle. I am in charge of writing [4.4](#), Flow Visualization and [4.5](#) Comparison of Results with Pre-Study Hypotheses and Literature. I assisted in the interpretation of results with a theoretical framework. I also created content for the results and analysis part in the presentation, including an analysis section that summarized all the results and made it presentable to an audience. I will also explain how our aerodynamic package's results compare to theory and literature. I present the results and analysis section of the presentation. My colleges helped me fine-tune the presentation's content.

Lars Petermeise I have attended all workshops and other mandatory tasks.

My main contribution during the postprocessing workshop were the graphics visualizing stream tubes on the sides of the front splitter, as well as the rear wing of the CFD model.

During the wind-tunnel building session I have supported in designing and fortifying the front splitter improvements.

Afterwards, during wind-tunnel testing, I have been responsible for operating the wind tunnel, which meant to set the different wind speeds, undergo emergency shut-off if required and to log all measured data for further processing.

For the report and presentation, I am responsible for the script that is the base for all calculations, visualizations and the resulting evaluation (it can be seen in [7.1](#)).

Karthik Tapasi Himanth I actively participated in all mandatory workshops and wind tunnel sessions throughout the project. During the CFD session, I successfully identified key streamlines in the post-processing phase, which played a crucial role in helping Valentine decide on the implementation of the ducktail modification.

In the building session, I assisted Erwan in constructing the front aerodynamic components of the model. During the wind tunnel session, I contributed by assisting the team with the attachment of aerodynamic devices to the vehicle before testing. For the report, I was responsible for writing Section [1](#) and Section [2](#) (The Figure [2](#) in Section [2.2](#) was done by me.) Regarding the presentation, I created the template and designed the overall layout. While Erwan determined the content flow and key ideas to be presented, I structured the slides and formatted the design accordingly.

Syuen Khor I attended all the mandatory workshops, CFD session and wind tunnel test. During post-processing, I contributed to the graphics visualization stream, working on the same computer as Lars to ensure our results matched those of Valentin and Erwan, who were working from another computer. I also verified that the results uploaded to Teams were accurate.

In the wind tunnel building session, I worked mainly on the rear modifications, where I was responsible for cutting the components and ensuring they fit properly.

During the wind tunnel test, my main task was to photograph and record videos of each configuration while the wind was active. Between the tests, I worked with the team to attach the modifications to the model and documented the process with behind-the-scenes photos, as well as images of the model after each modification. After the test, I organised and named the photos and videos according to the modifications and uploaded them on Teams.

For the report, I wrote sections [4.1](#), [4.2](#) and [4.3](#), while cooperating with Valentin for the subtopics in [4.2](#). Additionally, I wrote the entire conclusion (section [5](#)). I also reviewed the entire results section (section [4](#)) to ensure the clarity and accuracy, formulating the sentences when necessary.

Valentin Da Silva I attended all workshops and CFD simulations, using each team member's results to guide aerodynamic decisions. This allowed me to contribute to the initial car analysis and propose modifications.

During the building session, I suggested several aerodynamic devices, all discussed and validated by the team. My main focus was on the rear of the car: while Erwan extended the diffuser, I proposed adding a ducktail, and Eeshan and Karthik helped refine its shape based on CFD streamlines.

I also collaborated with Syuen, Erwan, and Risira on the design and attachment of the rear winglets.

Later, I suggested a concave bonnet shape to reduce drag from the cockpit opening, which was approved by the team.

During wind tunnel testing, Erwan and I secured the parts to the model. Thanks to Lars' precise wind tunnel control, the tests ran smoothly. I also documented our configurations with pictures (see [1](#) and for example all 4 pictures with [8c](#)).

For the report, I structured the entire document and contributed to [4.2](#) by expanding Syuen's work, adding [4.2.1](#) and [4.2.2](#). I also wrote [4.2.3](#) entirely and contributed to the first paragraph of [4.4](#).

Finally, I would like to thank the team and our teachers for making this project possible.